Materials Horizons

COMMUNICATION

View Article Online
View Journal

Cite this: DOI: 10.1039/c8mh00392k

Received 2nd April 2018,
Accepted 6th June 2018

DOI: 10.1039/c8mh00392k

rsc.li/materials-horizons

A siRNA-induced peptide co-assembly system as a peptide-based siRNA nanocarrier for cancer therapy†

Wenjun Li,[a] Dongyuan Wang,[a] Xiaodong Shi,[a] Jingxu Li,[a] Yue Ma,[a] Yanding Wang,[a] Tingting Li,[b] Jianing Zhang,[a] Rongtong Zhao,[a] Zhiqiang Yu,[c] Feng Yin *[a] and Zigang Li *[a]

Herein, we report a unique siRNA-induced peptide co-assembly nanocarrier, which could efficiently co-assemble upon the addition of siRNA, forming nanospheres with high biocompatibility and transfection efficiency both *in vitro* and *in vivo*. In a tumor xenograft nude mouse model, these siRNA–peptide nanospheres inhibited tumor volume growth by >60%.

Introduction

RNA interference (RNAi) is a widely used biological technology with high specificity and efficiency of gene knockdown.[1–5] However, to successfully survive ubiquitous RNAse and membrane barriers, an efficient siRNA application requires meticulously designed carriers.[6,7] Various nanomaterials,[8–12] including liposomes,[13] polymeric micelles,[14] and inorganic nanoparticles[15–18] have been developed for safe and efficient *in vivo* gene delivery. Nanomaterials based on both liposomes and polyethylenimine (PEI) are efficient siRNA carriers and have been widely used as commercial transfection reagents.[13] However, for *in vivo* siRNA delivery, specific and sometimes complicated modifications are usually required to obtain satisfactory biocompatibility.[19] Inorganic nanoparticles are also promising siRNA carriers due to their high transfection efficiency and low cell toxicity.[20] Despite these favorable properties, they are not degradable, a property that causes serious safety concerns, impeding their therapeutic applications. Therefore, the development of a novel siRNA nanocarrier with low cytotoxicity and high transfection efficiency is highly desirable and would be a great asset, both in research and in the clinic.

Conceptual insights

A novel and unique siRNA-induced peptide co-assembly nanocarrier with efficient RNA silencing efficiency is reported in this manuscript. This unique system showed high biocompatibility and low cytotoxicity both *in vitro* and *in vivo*. This system is based on peptides modified with a conceptual novel methionine modification strategy, which helps to increase the peptides' stability and helps the formation of peptide–nucleotide nanoparticles. The Met modification is reversible under a high concentration of GSH after cellular uptake to release the oligonucleotides. Besides, this novel peptide–nucleotide nanoparticle contains only nine amino acids, compared with other peptide carriers which generally contain over 20 amino acids and complicated modifications. This is the first successful attempt to apply stabilized peptides for gene delivery and could certainly add new thoughts for the peptide based bio-nanoparticles and fit the interests of the researchers working in this area.

As naturally biocompatible molecules, peptides can be rationally designed as efficient carriers for siRNA delivery.[21,22] The current, most commonly used peptide delivery systems can be divided into two basic categories: covalent linking or non-covalent linking. In a covalent linking delivery system, cell-penetrating peptides (CPPs) are conjugated with siRNA molecules to enable cellular uptake.[23,24] In non-covalent linking systems, the electrostatic interactions between the siRNA and CPPs or amphiphilic peptides can promote the formation of a stable complex and then cellular uptake.[25–30] For instance, Divita *et al.* developed an amphiphilic peptide, MPG, as an efficient siRNA carrier that is composed of the fusion domain from HIV-1 gp41 and the nuclear localization sequence (NLS) of SV40 T antigen.[31] Langel *et al.* also reported that a pH-titratable trifluoromethylquinoline modified peptide facilitates endosomal release.[32–34]

To achieve an appropriate peptide carrier, complicated modifications are usually required, including PEGylation, addition of β-cyclodextrin or a pH titratable group, *etc.* The peptides are typically longer than 20 amino acids.[25,26] We sought to develop a simple, stable, and efficient peptide-based nanocarrier. In the past decades, several research groups have developed various chemical

[a] State Key Laboratory of Chemical Oncogenomics, School of Chemical Biology and Biotechnology, Peking University Shenzhen Graduate School, Shenzhen, 518055, China. E-mail: lizg@pkusz.edu.cn; Fax: +86-755-2603-3174; Tel: +86-755-2603-3616

[b] School of Advanced Material, Peking University Shenzhen Graduate School, Shenzhen, 518055, China

[c] School of Pharmaceutical Sciences, Guangdong Provincial Key Laboratory of New Drug Screening, Southern Medical University, Guangzhou 510515, China

† Electronic supplementary information (ESI) available. See DOI: 10.1039/c8mh00392k

methodologies to stabilize peptides for different purposes. Most of the methodologies involve the chemical addition of a tether to the peptides,[35–42] improving the peptides' serum stability[43] and cell penetration capability.[44] Stabilized peptide ligands were developed to target various intracellular protein–protein interactions (PPI) for biological research and clinical trials.[45–57] In this study, for the first time, we utilized a novel Met cross-linking strategy to construct a peptide–siRNA co-assembly,[58,59] as shown in Fig. 1. The additional cross-linking on the Met brings two positive charges to the sulfonium center and can be reduced with the presence of GSH.[60] Taking the positive sulfonium centers into consideration, we envisioned that a suitable peptide stabilized using this method might be preferably induced by siRNA molecules to form a peptide–siRNA complex with high cellular uptake. Once the peptide–siRNA co-assembled nanoparticles are internalized by cells, the reduction of the cross-linking with the high concentration of intracellular GSH could eliminate redundant positive charges to weaken the electronic interaction between the peptide and siRNA molecules, thus promoting the release of the RNA. Based on this design, and after screening for suitable sequences, we herein report a novel and unique siRNA-induced peptide co-assembly system as an efficient gene nanocarrier.

Most peptide-based siRNA carriers require long sequences (>20 residues). After carrying out thorough screening, we identified peptide Fmoc-RRMEHRMEW, which is only composed of 9 amino acids. Two dedicatedly positioned Met residues were then stabilized with reducible cross-linkers to make the vector peptide Wpc, which is shown in Fig. 1. With an optimized peptide/siRNA ratio, peptide Wpc would spontaneously co-assemble upon the addition of siRNA to generate uniform peptide–siRNA nanospheres. AFM, SEM, DLS and *Z* potential measurements were utilized to further characterize the resulting peptide–siRNA co-assembly complex. The induced peptide–siRNA co-assembled nanospheres could efficiently deliver siRNA into different cell lines, including HeLa, Miacapa-2, PA-1, and A2780 cells, to specifically knockdown the target genes. In a tumor xenograft nude mouse model, the co-assembly-based nanoparticles showed efficient tumor growth of >60% *in vivo*. Notably, oligonucleotides other than siRNAs (such as: primer, plasmid, and aptamer) can also be co-assembled with Wpc peptide to form uniform nanospheres.

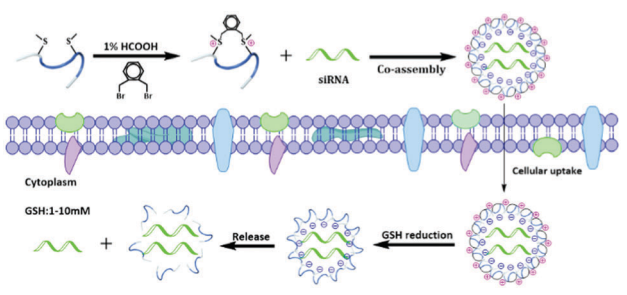

Fig. 1 Schematic presentation of the Wpc peptide with reducible cross-links, which can be induced to undergo co-assembly with siRNA to form nanoparticles for efficient siRNA transfection.

Results and discussion

Selected examples of peptides with different sequences and alkylation modifications are summarized in Table S1 (ESI†). We utilized gel retardation assays to evaluate the siRNA loading affinity of each peptide candidate. And we observed that peptide Wpc stood out with the highest siRNA loading ability, as can be seen in Fig. S1 (ESI†). The screening details are summarized in Fig. S1–S4 (ESI†).

Characterization by both atomic-force microscopy (AFM) and scanning electron microscopy (SEM) revealed that the peptide/siRNA complex appeared as a regular spherical structure with a diameter of around 200–300 nm, while Wpc itself was amorphous and highly soluble (Fig. 2A and B). Dynamic light scattering (DLS) analysis revealed that the hydrodynamic size of the peptide–siRNA complex was about ~390 nm (Fig. 2C). Furthermore, the results of the *Z* potential assay displayed a distinct decrease in the *Z* mV of peptide–siRNA nanoparticles compared to peptide alone, indicating the presence of siRNA in the nanospheres (Fig. 2D). When taken together, these results demonstrated that the peptide Wpc could be induced to co-assemble with siRNA to form a uniform and regular nanostructure. To further explore the stability of the peptide–siRNA nanoparticles in the tumor microenvironment and endosomes, the nanospheres were incubated in pH 5.5 HCl at 37 °C for 12 h and mouse serum for 5 h. Data from both the DLS analysis and SEM imaging showed negligible changes (Fig. S5–S7, ESI† and Fig. 2E). We then treated the peptide–siRNA co-assembled nanoparticles with 10 mM GSH at 37 °C for 12 h, mimicking the reductive conditions of the cytoplasm. We observed significant changes in both particle size and structure by DLS analysis (Fig. S8, ESI†) and SEM imaging (Fig. 2E). These results indicated that this siRNA nanocarrier might be satisfyingly stable in both the tumor microenvironment and endosomes while less stable in the reductive cytoplasm, thus promoting the release of the siRNA in the cell.

Flow cytometry assays were then utilized to evaluate the transfection efficiency of peptide Wpc in HeLa cells with Lipo-2000 and Oligo as positive controls (Fig. 2F and G). The mean fluorescence intensity and transfection efficiency analysis showed that the peptide–siRNA co-assembled nanoparticles could efficiently deliver siRNA into HeLa cells. Selected FACS results of other peptides are summarized in Fig. S9 (ESI†); most of them showed significantly lower siRNA loading ability and transfection efficiency when compared with peptide Wpc, except for two peptides that showed high transfection but exhibited significant cytotoxicity. Confocal microscopy imaging was used to further confirm the cellular uptake efficiency of Wpc peptide–siRNA nanoparticles in HeLa cells (Fig. 2H). Strong fluorescence signals were homogeneously distributed in the peptide–siRNA treated cells, whereas only negligible fluorescence signals were observed from HeLa cells treated with PBS and free siRNA^{FAM}, while the fluorescence signals from the commercially acquired transfection reagent, Lipo-2000 and Oligo, were also notably weaker than those with the peptide–siRNA nanoparticles. Notably, homogeneously-distributed and strong fluorescent signals could be observed within the entire cytoplasm of the HeLa cells after only

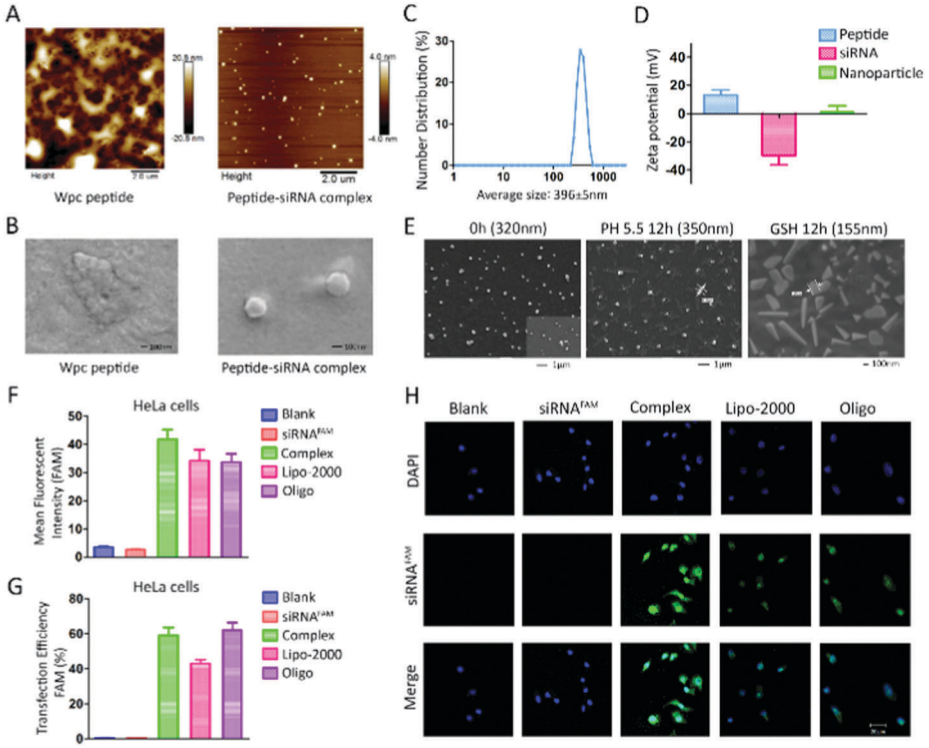

Fig. 2 Characterization and cell transfection efficiency analysis of the peptide–siRNA nanoparticles. (A) AFM character of the Wpc peptide and peptide–siRNA complex. (B) SEM character of the Wpc peptide and peptide–siRNA complex. The peptide has no visible structure in the AFM and SEM images. And both the AFM and SEM images showed homogeneous and clear co-assembled nanoparticles of peptide–siRNA with about 200–300 nm diameter. (C) DLS analysis of the peptide–siRNA co-assembly complex. The particle size of the peptide–siRNA complex was uniform with an average diameter of about 396 nm. (D) *Z* potential analysis of the peptide–siRNA co-assembly complex. (E) SEM image of the peptide–siRNA co-assembled nanoparticles incubated with pH 5.5 HCl and 10 mM GSH at 37 °C for 12 h. No obvious change in the co-assembled nanoparticles was observed at pH = 5.5 for 12 h, while significant degradation can be observed when incubated with 10 mM GSH for 12 h. (F and G) Mean fluorescence intensity and transfection efficiency of the peptide–siRNA co-assembled nanoparticles (2.0 μg siRNA with 50 μg peptide for HeLa cells with 40% density) in HeLa cells. Both the mean fluorescence intensity and transfection efficiency analysis showed that the peptide–siRNA co-assembled nanoparticles can efficiently delivery siRNA into HeLa cells. (H) Confocal microscopy image of peptide Wpc, Lipo-2000 and Oligo loading with $siRNA^{FAM}$. The image of the peptide–siRNA complex (2.0 μg siRNA with 50 μg peptide) showed a significant internalization of peptide–siRNA nanoparticles. The scale bars are 20 μm. All the experiments were conducted twice with consistent results. Error bars represent SD of data. The statistical differences between the control group and experimental groups were analyzed by one-way ANOVA.

20 minutes of treatment with the peptide–$siRNA^{FAM}$ co-assembly complex (Fig. S10, ESI†).

The Survivin gene is an important survival regulator for HeLa cells,[61,62] and we utilized Survivin siRNA as a proof-of-concept model in order to study the efficiency of our peptide-based nanocarrier. RT-PCR was first used to evaluate the gene knockdown efficiency in HeLa cells. After transfection of the peptide–siRNA co-assembly complex (2.0 μg siRNA with 50 μg peptide) for 48 h, the mRNA level of Survivin significantly decreased compared to the negative controls (Fig. 3A). The gene knockdown efficiency for this co-assembly vector was further confirmed by the delivery of Bcl-2 siRNA into HeLa cells, which showed a similar knockdown efficiency to Survivin (Fig. 3B). Meanwhile, RT-PCR analysis of other screened peptide–Survivin siRNA complexes was also performed in HeLa cells, and all of the peptides showed significantly lower gene knockdown efficiency compared to that of Wpc (Fig. S11, ESI†). The transfection efficiency was further proved using other siRNAs with different cancer cell lines, including K-ras siRNA in Miacapa-2 cells, LSD-1 siRNA in PA-1 cells, and HDAC-1 siRNA in A2780 cells (Fig. 3C and Fig. S12, ESI†).

HEK-293T cells, QSG7701 human liver cells, and HeLa cells were then tested in MTT assays to evaluate the cytotoxicity of the Wpc peptide. The results showed that negligible cytotoxicity was detected for all cell lines (Fig. 3D). Blood toxicity assays were also performed at 37 °C with 10^7–10^8 fresh mouse blood cells, with only negligible hemocytotoxicity observed (Fig. 3F and Fig. S13, ESI†). These results demonstrated that this peptide based nanocarrier is biocompatible with low cytotoxicity and hemocytotoxicity, indicating that it has promising potential for *in vivo* applications. Additionally, growth inhibition of HeLa cells was observed 48 h after the introduction of a peptide–Survivin siRNA complex (Fig. 3E). In cell cycle arrestment analysis, both the peptide–Survivin siRNA complex and Survivin siRNA delivered by positive controls (Lipo-2000 and Oligo) showed clear G2 phase cycle arrest (Fig. 3G).[63,64] This result hints that our novel peptide–siRNA nanoparticles have potential anti-tumor bioactivity.

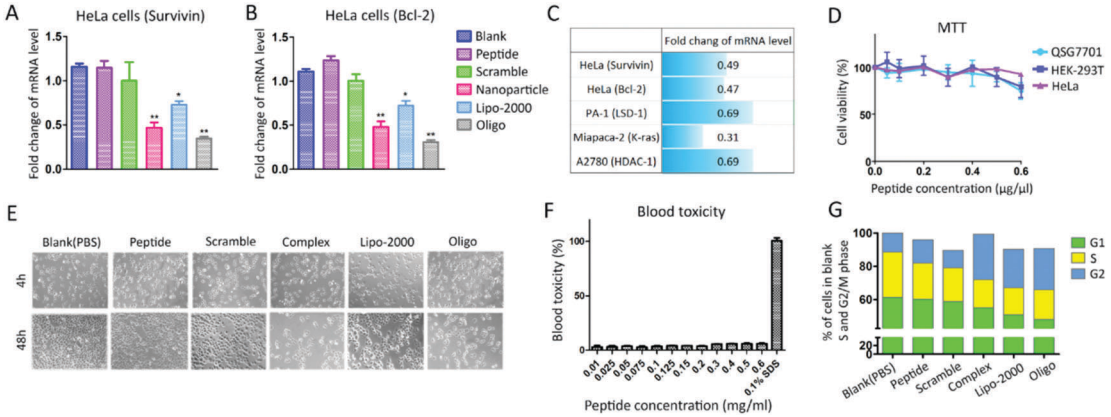

Fig. 3 Cell assay evaluation of the peptide–siRNA co-assembled nanoparticles. Scramble: peptide–siRNA (Scramble) complex. (A) RT-PCR analysis of HeLa cells transfected with peptide–siRNA (Survivin) co-assembled nanoparticles. (B) RT-PCR analysis of HeLa cells transfected with peptide–siRNA (Bcl-2) co-assembled nanoparticles. Both the delivery of Survivin and Bcl-2 siRNA showed a significant knockdown in HeLa cells. * $P < 0.05$, ** $P < 0.01$ *vs.* PBS (blank). (C) The summary of the fold change of the mRNA level in different cell lines by RT-PCR analysis (HeLa cells, PA-1 cells, Miapaca-2 cells and A2780 cells), transfected with different peptide–siRNA nanoparticles. The detailed RT-PCR results are provided in Fig. S12 (ESI†). (D) MTT assay of peptide Wpc in Immortalized cells (HEK-293T cells), normal liver cells (QSG7701 cells) and tumor cells (HeLa cells). (E) Inverted microscope image of HeLa cells treated with peptide siRNA co-assembled nanoparticles after 4 h and 48 h. (F) Blood cytotoxicity assay of peptide Wpc in fresh mouse blood with 0.1% SDS as a positive control. (G) Percentage of HeLa cells in each mitotic phase after being treated with different samples. HeLa cells were transfected with (2.0 μg siRNA with 50 μg peptide) nanoparticles for 48 h. Then they were stained and analyzed by flow cytomerty. A clearly higher proportion of HeLa cells were in the G2 phase after being treated with peptide–siRNA nanoparticles or positive controls than any other treatments. All the experiments were conducted twice with consistent results. Error bars represent SD of the data. The statistical differences between the control group and experimental groups were analyzed by one-way ANOVA.

Then we examined the tumor growth inhibition of the peptide–siRNA co-assembled nanoparticles in a HeLa tumor xenograft nude mouse model (Fig. 4). After intratumor injection for 20 days (0.32OD siRNA per mice, once every 2 days), a significant reduction in tumor volume was observed in the mice treated with the peptide–siRNA (Survivin) nanocomplex, with an inhibition rate of 60% (Fig. 4A and B). The immunohistochemistry analysis further showed the gene knockdown efficiency of the peptide–siRNA nanocomplex and the up-regulation of tunnel and caspase-3 in tumor tissues (Fig. 4C). Moreover, there was no obvious weight loss in mice treated with the peptide–siRNA co-assembled nanoparticles during the examination period, indicating the low toxicity of our peptide–siRNA nanocomplex (Fig. S14, ESI†). We further monitored the body distribution imaging of the peptide–siRNA co-assembly complex by a small animal *in vivo* imaging system (CRI Maestro, USA) (Fig. S15 and S16, ESI†). After intratumor injection, mice were imaged at different time points (0 h, 10 min, 1 h, 4 h, 8 h, and 24 h). Observation of the

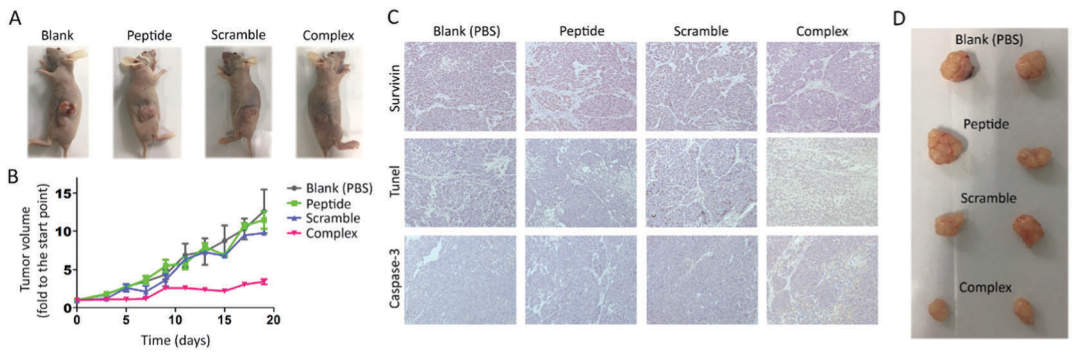

Fig. 4 Antitumor activities of peptide–siRNA co-assembled nanoparticles in a xenograft nude mice model of HeLa cells. Scramble: peptide–siRNA (Scramble) complex; complex: peptide–siRNA (Survivin) complex. (A) Photograph of the representative mice at day 19. (B) Change of tumor volume with time. The peptide–siRNA nanoparticles inhibited the growth of the tumor with the smallest size and volume of tumor. Relative tumor volume was calculated as *V*/*V* blank (day 0), where *V* represent the volume on a particular day, respectivly. Error bars represent SEMs for three independent datasets. Mean tumor volumes were analyzed using one-way ANOVA. Values represent the means ± SD, $n = 4–6$ tumors. *: for the group of scramble, two mice were found to be dead at day 11, due to the malignancy of the tumor, so there is only one mouse remaining. (C) Immunohistochemistry analysis of the cervical carcinomas collected from different groups of mice after 3 weeks of treatment. Down-regulation of the Survivin protein level in cervical carcinomas further induced the high expression of Tunel and Caspase-3. Survivin protein exhibited relatively high expression in normal cervical carcinomas and groups treated with peptide only and peptide–scramble nanoparticles. The immunohistologic staining of human cervical tumor tissues was performed with anti-Survivin, anti-Tunel and anti-Caspase-3. MicroSpot focusing objective, 20×. (D) Representative tumor tissue images of mice treated with PBS, peptide only, Scramble and peptide–siRNA nanoparticles.

fluorescent images revealed that the co-assembled nanoparticles accumulated in the tumor constantly for at least 24 h. Furthermore, the images of other organs (heart, liver, spleen, lung, kidney, brain, and tumor) showed little presence of the peptide–siRNA complexes, indicating clearly that they were mostly accumulated in the tumor (Fig. S17, ESI†). Lastly, HE staining from each organ of the mice treated with the peptide–siRNA complex showed no more obvious abnormality than the other groups (Fig. S18, ESI†). These results demonstrated that this novel peptide–siRNA co-assembly-based nanocarrier could be utilized for *in vivo* siRNA delivery with high efficiency and low toxicity, which can serve as a potential siRNA-based anti-tumor therapy.

Conclusions

In summary, we have developed a novel and unique siRNA-induced peptide co-assembly system for cancer therapy both *in vitro* and *in vivo*. We envisioned that a peptide stabilized with a reducible sulfonium linker could efficiently co-assemble with siRNA, and that the reduction of crosslinking in the cytoplasm could help to release the free siRNA to further promote RNA interference. After designing various peptides and screening them, we found that the peptide Wpc could spontaneously co-assemble with siRNA to form regular nanospheres and deliver the siRNA into different cell lines, efficiently knocking down the target gene. In a xenograft nude mice model of HeLa cells, the peptide–siRNA nanoparticles reduced the tumor volume by 60% on average, with negligible evidence of toxicity *in vivo*. These results demonstrated that this novel peptide–siRNA co-assembly system could be utilized for siRNA delivery both *in vitro* and *in vivo*.

After many years of debate concerning siRNA druggability, the first RNAi therapeutic, Patisiran, was approved very recently.[65] This encouraging response will surely promote the therapeutic development of siRNAs. From the early 21st century, the main hurdle facing RNAi therapeutics has always been the lack of efficient and biocompatible delivery vectors. In this report, we rationally designed and screened for a unique siRNA-induced peptide co-assembly nanocarrier possessing both high biocompatibility and high efficiency. Compared with the other peptide-based siRNA vectors that have been reported, this strategy is simpler, needing only a 9-residue peptide and one facile modification step. Furthermore, the peptide's charge has been neutralized to be only +1 after intracellular reduction so as to avoid unspecific cytotoxicity and possible immune responses.[66,67] The assembly process is spontaneous upon the addition of siRNA and the resulting peptide–siRNA complex is uniform and evenly distributed in the solution.

After designing and screening various peptides and their Met modified derivatives, we found the additional positive charges generated by Met *S*-alkylation could help the siRNA incorporation. The cyclic *S*-alkylated peptide (w-ph-c) was constrained and the positive charges might be positioned more preferably for siRNA loading comparing to its linear dual *S*-alkylated analogue (w-ph). Of course, an efficient co-assembly of siRNA and peptides is a synergetic result of various factors, including suitable peptide sequences and lipophilicity. Further optimization of this siRNA induced peptide co-assembly nanocarrier is under current investigation. We believe that specially designed linkers, conformational alignments of amino acids and addition of unnatural amino acids will surely provide us with more efficient and biocompatible delivery vectors and help to advance the therapeutic applications of siRNAs.

Experimental section

S-Alkylated peptide preparation

The peptide was synthesized by standard Fmoc-based solid phase peptide synthesis (SPPS) and purified by HPLC and identified by LC-MS. 2 mg of purified peptide was dissolved in 3 ml of ddH_2O. Then 5 mg of alkylation reagent (for 1,2-xylene alkylation, we used 1,2-bis(bromomethyl)benzene) and 30 μl of HCOOH were added and the mixture was shaken for 18 h at room temperature. After that we used HPLC to seprate the *S*-alkylated peptide and used LC-MS to identify the *S*-alkylated product.

Gel retardation

The screened peptides (dissolved in DEPC water) were qualified by their weight. As for the peptide whose sequence contains a W amino acid, we used nanodrop to qualify its concentration in DEPC water at the absorption at 280 nm. The screened peptides were incubated with siRNA (0.4 μg) in RNAase free tubes at room temperature for 10 min, with a gradient concentration. Then 1% agarose gel 110 V electrophoresis was performed for 15 min in TAE buffer solution with 40 mM Tris–HCl, 1% acetic acidv/v, and 1 mM ethylene diamine tetraacetic acid (EDTA). Golden View was used to stain the agarose gel to visualize the retardation of the peptide–siRNA complex and the gel was further analyzed by a UV illuminator to compare the position of the peptide–siRNA complex and free siRNA. The final mass ratio between peptide and siRNA is 25 μg : 1 μg.

AFM (atomic-force microscopy)

Peptide Wpc was incubated with siRNA (0.4 μg) in an RNAse free tube at room temperature for 10 min. ddH_2O was added to dilute the solution, and then a pipettor was used to transfer 20 μl to the surface of single mica for spin-coating. Finally, the peptide–siRNA co-assembled nanoparticles homogeneously distributed on the surface of single mica were analyzed by AFM.

SEM (scanning electron microscopy)

Peptide Wpc was incubated with siRNA (0.4 μg) in an RNAse free tube at room temperature for 10 min. ddH_2O was added to dilute the solution, and a pipettor was used to transfer 30 μl to the surface of silicon. After drying at 60 °C, the peptide–siRNA co-assembled nanoparticles on the surface of silicon were analyzed by SEM.

siRNA transfection

HeLa cells, Miacapa-2 cells, PA-1 cells or A2780 cells (30% density) were washed with PBS 3 times and the medium was

replaced with an Opti-MEM medium (500 μl) without FBS and PS for 1 h. After 2.0 μg functional siRNA and 50 μg peptide were slightly mixed for 10 min, the co-assembled nanoparticles were added to medium and slightly mixed. After being cultured at 37 °C, 5% CO_2 for 5 h, 10% FBS and 1% PS were added to the medium and culturing was continued for 48 h. (After 24 h, 500 μl fresh medium could be added for cell growth). Then the cells were washed with PBS 2 times, and RNA was extracted for subsequent reverse transcription and real-time PCR analysis.

Flow cytometry analysis

HeLa cells were culture in DMEM medium with 10% FBS (v/v) at 37 °C, in a 5% CO_2 incubator. HeLa cells (40% density) were washed with PBS and then incubated with Opti-MEM medium without FBS and PS for 1 h. After 2.0 μg $siRNA^{FAM}$ and 50 μg peptide were slightly mixed for 10 min, the FAM labelled siRNA–peptide co-assembled nanoparticles were slightly added to the medium and mixed. Then HeLa cells were cultured at 37 °C, 5% CO_2 for 3 h. After washing with PBS 3 times, trypsin digestion (1 min), and re-suspension (500 μl) in PBS, cellular fluorescence was analyzed using a BD FACSCalibur flow cytometer. The mean intracellular fluorescence intensity was analyzed by Flowjo 7.6.1 software. The values represent averages of three independent experiments.

Confocal microscopy image

HeLa cells (40% density) were washed with PBS 2 times and later incubated with Opti-MEM medium without FBS and PS for 1 h. After 2.0 μg $siRNA^{FAM}$ and 50 μg peptide were slightly mixed for 10 min, the peptide–siRNA nanoparticles were slightly added in the medium and further incubated at 37 °C, 5% CO_2 for 3 h. After washing with PBS at least 3 times, the cells were fixed with 4% formaldehyde (Alfa Aesar, MA) for 20 min at room temperature. Then the cells were washed with PBS another 3 times for further staining by 1 μg ml^{-1} 4′,6-diamidino-2-phenylindole (DAPI) (Invitrogen, CA) for 10 min. Finally the cells were imaged by confocal microscopy.

RNA extraction and real-time PCR analysis

After transfecting with peptide–siRNA nanoparticles for 48 h, TRIzol reagent (Invitrogen) was used to extract the RNA from the HeLa cells and a spectrophotometer (Nano-Drop ND-2000) was used to quantify the amount of extracted RNA. Then based on the amount of RNA, reverse transcription reagent was used to transcribe the mRNA to cDNA: total RNA (2 μg) and a commercial reverse transcriptase kit from Promega were mixed and reacted at 42 °C for 1 h according to the instructions. Finally, the fold change of the mRNA level was analyzed by a real-time PCR system with SYBR green dye according to the cDNA from reverse transcription.

Cell viability test

HeLa cells (30% density) were transfected with peptide–siRNA (Survivin) nanoparticles. 4 h later, the cells were imaged by Inverted microscope. And at 24 h, the cells were washed with PBS, digested with trypsin and re-cultured in fresh medium for another 24 h and imaged by Inverted microscope to compare the anti-growth effect of the peptide–siRNA nanoparticles.

Cytotoxicity test

MTT assay: 8000 cells were cultured in 96-wells plate. After being washed with PBS and changed with fresh medium without FBS, different concentrations of samples were added to the plate and incubated at 37 °C, 5% CO_2 for 2 h. Then 10% FBS and 1% PS were added and culturing of the cells was continued for 24 h. Then a CCK-8 kit was used to evaluate the cell viability by comparison of the absorption at 450 nm.

Blood toxicity assay

Fresh mouse blood was collected from BALB/c mice, and 10 μl of 10 mg ml^{-1} heparin sodium was added immediately. Then 1 ml of the whole blood was centrifuged at 1500 rad for 10 min to isolate RBCs from blood and further washed with PBS 2 times until the supernate was not red anymore. Then 200 μl of fresh blood cells was diluted with 8 ml PBS. To test the blood toxicity of the peptide, different concentrations of peptide (from 0.01 μg μl^{-1} to 0.6 μg μl^{-1}) were added to 0.5 ml of diluted fresh blood cells (about 1×10^8 cells per ml) respectively with 0.1% SDS as a positive control. These mixtures were placed on a shaker in an incubator at 37 °C for 1.5 h. Then after centrifugation, the supernate of each sample was taken to measure its absorbance at 540 nm and 655 nm (as a contrast) by an iMark microplate reader (BioRad, Hercules, CA).

Cell cycle assay

HeLa cells (30% density) were transfected with peptide–siRNA (Survivin) nanoparticles. After being cultured at 37 °C, 5% CO_2 for 5 h, 10% FBS and 1% PS were added to the medium and culturing was continued for 48 h (at 24 h, the cells are washed with PBS, digested with trypsin and re-cultured in fresh medium). Then they were digested and stained with 70% ethanol at 4 °C for 4 h. After centrifugation and washing with PBS, the cells were stained with a mixture of 20 μl 10% Triton, 1 μl (10 mg ml^{-1}) RNase, 5 μl (1 mg ml^{-1}) PI and 200 μl PBS at 37 °C for 30 min. Lastly, the cell cycle of HeLa cells transfected with nanoparticles was analyzed by flow cytomery.

Animal experimennts

Athymic nude mice (BALB/c ASlac-nu, 4 weeks old) were obtained from Vital River Laboratory Animal Technology Co. Ltd of Beijing, People's Republic of China and allowed an acclimation period of 1 week. Mice were maintained in an isolated biosafety facility for specific pathogen free (SPF) animals with bedding, food and water. All operations were carried out in accordance with the National Standard of Animal Care and Use Procedures at the Laboratory Animal Center of Peking University Shenzhen Graduate School, Guangdong Province, People's Republic of China (the permit number is IACUC-ER-0023-005).

In vivo mice imaging

When the HeLa tumor volume of the mice reached approximately 200–300 mm^3, the mice were intratumorally injected

with 80 μl of peptide–siRNA^{cy3} nanoparticles (2 μg siRNA^{cy3} + 50 μg peptide). After being anesthetized with isoflurane (5% isoflurane/1 L O_2 concentration for the first time and 2–3% isoflurane/1 L air concentration for maintenance), the mice were immediately imaged to monitor the distribution of peptide–siRNA nanoparticles *in vivo* at each time point (10 min, 1 h, 4 h, 8 h, 12 h and 24 h). In this study, the imaging system is an *ex/in vivo* imaging system (CRI Maestro, USA) (ex: 704 nm; filter: 735 nm).

Preparation for paraffin section histological analysis (IHC)

Organ tissues for histological analysis were all collected from the final day in the mice experiments. Organ tissues were fixed in 4% formalin–saline at room temperature for 24 h. Subsequently, the tissues were embedded in paraffin blocks and 4 mm thick paraffin sections were installed on glass slides for hematoxylin and eosin (H&E) staining and later examined by light microscopy (Olympus BX51). As for immunohistochemistry analysis, cervix carcinoma tissue sections were firstly immersed in 3% H_2O_2 for 5 minutes. Then 5% BSA was used to block the nonspecific binding sites of the tissue for 15 min. Diluted antibody against Survivin was incubated with the slides at 4 °C overnight, followed by washing and incubating with the Rabbit-probe HRP-polymer detection system, based on the instructions from the supplier. Finally, the slides were incubated with 3,3′-diaminobenzidine substrate and counterstained with hematoxylin, according to the ImmPACT DAB Peroxidase Substrate Kit (Vector Laboratories) for 4 min.

Conflicts of interest

There are no conflicts to declare.

Acknowledgements

We acknowledge financial support from the Natural Science Foundation of China grants 21778009 and 81701818; MOST 2015DFA31590; and the Shenzhen Science and Technology Innovation Committee, JCYJ20170412150609690, KQJSCX2017-0728101942700 and JCYJ20170807144449135. This work is supported by High-Performance Computing Platform of Peking University.

References

1 D. H. Kim and J. J. Rossi, *Nat. Rev. Genet.*, 2007, **8**, 173.
2 D. Bumcrot, M. Manoharan, V. Koteliansky and D. W. Sah, *Nat. Chem. Biol.*, 2006, **2**, 711.
3 N. Nayerossadat, T. Maedeh and P. A. Ali, *Adv. Biomed. Res.*, 2012, **1**, 27.
4 K. A. Whitehead, R. Langer and D. G. Anderson, *Nat. Rev. Drug Discovery*, 2009, **8**, 129.
5 S. F. Dowdy, *Nat. Biotechnol.*, 2017, **35**, 222.
6 F. Mingozzi and K. A. High, *Nat. Rev. Genet.*, 2011, **12**, 341.
7 P. D. Robbins and S. C. Ghivizzani, *Pharmacol. Ther.*, 1998, **80**, 35.
8 H. Yin, R. L. Kanasty, A. A. Eltoukhy, A. J. Vegas, J. R. Dorkin and D. G. Anderson, *Nat. Rev. Genet.*, 2014, **15**, 541.
9 C. Gehin, J. Montenegro, E. K. Bang, A. Cajaraville, S. Takayama, H. Hirose, S. Futaki, S. Matile and H. Riezman, *J. Am. Chem. Soc.*, 2013, **135**, 9295.
10 Q. Chen, J. Chen, C. Liang, L. Feng, Z. Dong, X. Song, G. Song and Z. Liu, *J. Controlled Release*, 2017, **263**, 79.
11 C. Liang, L. Xu, G. Song and Z. Liu, *Chem. Soc. Rev.*, 2016, **45**, 6250.
12 J. G. Boorn, M. Schlee, C. Coch and G. Hartmann, *Nat. Biotechnol.*, 2011, **29**, 325.
13 C. Wolfrum, S. Shi, K. N. Jayaprakash, M. Jayaraman, G. Wang, R. K. Pandey, K. G. Rajeev, T. Nakayama, K. Charrise, E. M. Ndungo, T. Zimmermann, V. Koteliansky, M. Manoharan and M. Stoffel, *Nat. Biotechnol.*, 2007, **25**, 1149.
14 S. Dinçer, M. Türk and E. Pişkin, *Gene Ther.*, 2005, **12**, 139.
15 R. Kanasty, J. R. Dorkin, A. Vegas and D. Anderson, *Nat. Mater.*, 2013, **12**, 967.
16 P. Ghosh, G. Han, M. De, C. K. Kim and V. M. Rotello, *Adv. Drug Delivery Rev.*, 2008, **60**, 1315.
17 P. Guo, O. Coban, N. M. Snead, J. Trebley, S. Hoeprich, S. Guo and Y. Shu, *Adv. Drug Delivery Rev.*, 2010, **62**, 650.
18 Y. Lei, L. Tang, Y. Xie, Y. Xianyu, L. Zhang, P. Wang, Y. Hamada, K. Jiang, W. Zheng and X. Jiang, *Nat. Commun.*, 2017, **8**, 15130.
19 Y. C. Tseng, S. Mozumdar and L. Huang, *Adv. Drug Delivery Rev.*, 2009, **61**, 721.
20 F. Yin, C. Yang, Q. Wang, S. Zeng, R. Hu, G. Lin, J. Tian, S. Hu, R. Lan, H. Yoon, F. Lu, K. Wang and K. Yong, *Theranostics*, 2015, **5**, 818.
21 A. Eguchi, B. R. Meade, Y. C. Chang, C. T. Fredrickson, K. Willert, N. Puri and S. F. Dowdy, *Nat. Biotechnol.*, 2009, **27**, 567.
22 A. T. Jones and E. J. Sayers, *J. Controlled Release*, 2012, **161**, 582.
23 E. Jin, B. Zhang, X. Sun, Z. Zhou, X. Ma, Q. Sun, J. Tang, Y. Shen, E. Van Kirk, W. J. Murdoch and M. Radosz, *J. Am. Chem. Soc.*, 2013, **135**, 933.
24 L. Crombez, G. Aldrian-Herrada, K. Konate, Q. N. Nguyen, G. K. McMaster, R. Brasseur, F. Heitz and G. Divita, *Mol. Ther.*, 2009, **17**, 95.
25 L. Crombez, M. C. Morris, S. Dufort, G. Aldrian-Herrada, Q. Nguyen, G. Mc Master, J. L. Coll, F. Heitz and G. Divita, *Nucleic Acids Res.*, 2009, **37**, 4559.
26 M. C. Morris, E. Gros, G. Aldrian-Herrada, M. Choob, J. Archdeacon, F. Heitz and G. Divita, *Nucleic Acids Res.*, 2007, **35**, e49.
27 H. Margus, K. Padari and M. Pooga, *Mol. Ther.*, 2012, **20**, 525.
28 B. R. Meade and S. F. Dowdy, *Adv. Drug Delivery Rev.*, 2007, **59**, 134.
29 T. Endoh and T. Ohtsuki, *Adv. Drug Delivery Rev.*, 2009, **61**, 704.
30 F. Simeoni, M. Morris, F. Heitz and G. Divita, *Nucleic Acids Res.*, 2003, **31**, 2717.
31 S. E. Andaloussi, T. Lehto, I. Mager, K. Rosenthal-Aizman, I. I. Oprea, O. E. Simonson, H. Sork, K. Ezzat, D. M. Copolovici, K. Kurrikoff, J. R. Viola, E. M. Zaghloul, R. Sillard, H. J. Johansson,

F. Said Hassane, P. Guterstam, J. Suhorutsenko, P. M. Moreno, N. Oskolkov, J. Halldin, U. Tedebark, A. Metspalu, B. Lebleu, J. Lehtio, C. I. Smith and U. Langel, *Nucleic Acids Res.*, 2011, **39**, 3972.

32 R. Sheng, T. Luo, Y. Zhu, H. Li, J. Sun, S. Chen, W. Sun and A. Cao, *Biomaterials*, 2011, **32**, 3507.

33 P. M. Klein, S. Reinhard, D.-J. Lee, K. Müller, D. Ponader, L. Hartmann and E. Wagner, *Nanoscale*, 2016, **8**, 18098.

34 A. Gandioso, A. Massaguer, N. Villegas, C. Salvans, D. Sanchez, I. Brun-Heath, V. Marchan, M. Orozco and M. Terrazas, *Chem. Commun.*, 2017, **53**, 2870.

35 G. J. Hilinski, Y.-W. Kim, J. Hong, P. S. Kutchukian, C. M. Crenshaw, S. S. Berkovitch, A. Chang, S. Ham and G. L. Verdine, *J. Am. Chem. Soc.*, 2014, **136**, 12314.

36 N. E. Shepherd, H. N. Hoang, G. Abbenante and D. P. Fairlie, *J. Am. Chem. Soc.*, 2005, **127**, 2974.

37 A. Muppidi, K. Doi, S. Edwardraja, E. J. Drake, A. M. Gulick, H. G. Wang and Q. Lin, *J. Am. Chem. Soc.*, 2012, **134**, 14734.

38 J. W. Checco, E. F. Lee, M. Evangelista, N. J. Sleebs, K. Rogers, A. Pettikiriarachchi, N. J. Kershaw, G. A. Eddinger, D. G. Belair, J. L. Wilson, C. H. Eller, R. T. Raines, W. L. Murphy, B. J. Smith, S. H. Gellman and W. D. Fairlie, *J. Am. Chem. Soc.*, 2015, **137**, 11365.

39 D. Sadowsky, M. A. Schmitt, H.-S. Lee, N. Umezawa, S. Wang, Y. Tomita and S. H. Gellman, *J. Am. Chem. Soc.*, 2005, **127**, 11966.

40 G. M. Fang, J. X. Wang and L. Liu, *Angew. Chem., Int. Ed.*, 2012, **51**, 10347.

41 T. S. Haque, J. C. Little and S. H. Gellman, *J. Am. Chem. Soc.*, 1994, **116**, 4105.

42 H. K. Cui, Y. Guo, Y. He, F. L. Wang, H. N. Chang, F. M. Wu, C. L. Tian and L. Liu, *Angew. Chem., Int. Ed.*, 2013, **52**, 9558.

43 G. H. Bird, W. C. Crannell and L. D. Walensky, *Curr. Protoc. Chem. Biol.*, 2011, **3**, 99.

44 Y. Tian, X. Zeng, J. Li, Y. Jiang, H. Zhao, D. Wang, X. Huang and Z. Li, *Chem. Sci.*, 2017, **8**, 7576.

45 C. E. Schafmeister, J. Po and G. L. Verdine, *J. Am. Chem. Soc.*, 2000, **122**, 5891.

46 A. M. Spokoyny, Y. Zou, J. J. Ling, H. Yu, Y.-S. Lin and B. L. Pentelute, *J. Am. Chem. Soc.*, 2013, **135**, 5946.

47 T. E. Speltz, S. W. Fanning, C. G. Mayne, C. Fowler, E. Tajkhorshid, G. L. Greene and T. W. Moore, *Angew. Chem., Int. Ed.*, 2016, **55**, 4252.

48 P. M. Cromm, J. Spiegel, P. Kuchler, L. Dietrich, J. Kriegesmann, M. Wendt, R. S. Goody, H. Waldmann and T. N. Grossmann, *ACS Chem. Biol.*, 2016, **11**, 2375.

49 G. Lautrette, F. Touti, H. G. Lee, P. Dai and B. L. Pentelute, *J. Am. Chem. Soc.*, 2016, **138**, 8340.

50 M. Pelay-Gimeno, A. Glas, O. Koch and T. N. Grossmann, *Angew. Chem., Int. Ed.*, 2015, **54**, 8896.

51 Y. Tian, J. X. Li, H. Zhao, X. Z. Zeng, D. Y. Wang, Q. S. Liu, X. G. Niu, X. H. Huang, N. H. Xu and Z. G. Li, *Chem. Sci.*, 2016, **7**, 3325.

52 H. Zhao, Q. S. Liu, H. Geng, Y. Tian, M. Cheng, Y. H. Jiang, M. S. Xie, X. G. Niu, F. Jiang and Y. O. Zhang, *Angew. Chem., Int. Ed.*, 2016, **55**, 12088.

53 K. Hu, H. Geng, Q. Zhang, Q. Liu, M. Xie, C. Sun, W. Li, H. Lin, F. Jiang, T. Wang, Y. D. Wu and Z. Li, *Angew. Chem., Int. Ed.*, 2016, **55**, 8013.

54 M. Xie, H. Zhao, Q. Liu, Y. Zhu, F. Yin, Y. Liang, Y. Jiang, D. Wang, K. Hu, X. Qin, Z. Wang, Y. Wu, N. Xu, X. Ye, T. Wang and Z. Li, *J. Med. Chem.*, 2017, **60**, 8731.

55 S. Hyun, Y. Choi, H. N. Lee, C. Lee, D. Oh, D.-K. Lee, C. Lee, Y. Lee and J. Yu, *Chem. Sci.*, 2018, **9**, 3820.

56 S. Jang, S. Hyun, S. Kim, S. Lee, I. S. Lee, M. Baba, Y. Lee and J. Yu, *Angew. Chem., Int. Ed.*, 2014, **53**, 10086.

57 J. Pai, T. Yoon, N. D. Kim, I. S. Lee, J. Yu and I. Shin, *J. Am. Chem. Soc.*, 2012, **134**, 19287.

58 T. J. Deming, *Bioconjugate Chem.*, 2017, **28**, 691.

59 J. R. Kramer and T. J. Deming, *Chem. Commun.*, 2013, **49**, 5144.

60 X. Shi, R. Zhao, Y. Jiang, H. Zhao, Y. Tian, Y. Jiang, J. Li, W. Qin, F. Yin and Z. Li, *Chem. Sci.*, 2018, **9**, 3227.

61 S. Hendruschk, R. Wiedemuth, A. Aigner, K. Topfer, M. Cartellieri, D. Martin, M. Kirsch, C. Ikonomidou, G. Schackert and A. Temme, *Neuro-Oncology*, 2011, **13**, 1074.

62 M. Pennati, M. Folini and N. Zaffaroni, *Carcinogenesis*, 2007, **28**, 1133.

63 Y. Li, D. Liu, Y. Zhou, Y. Li, J. Xie, R. J. Lee, Y. Cai and L. Teng, *J. Cancer*, 2015, **6**, 1187.

64 Z. Wenying, J. Zhaoning, Y. Zhimin, C. Dongyun and S. Lili, *Cell Biochem. Biophys.*, 2012, **62**, 337.

65 C. R. Lindenboom and J. Brodsky, FDA Grants Alnylam Breakthrough Therapy Designation (BTD) for Patisiran for the Treatment of Hereditary ATTR (hATTR) Amyloidosis with Polyneuropathy, http://investors.alnylam.com/news-releases/news-release-details/us-food-and-drug-administration-fda-grants-alnylam-breakthrough, Nov. 2017.

66 J. Li, X. Yu, Y. Wang, Y. Yuan, H. Xiao, D. Cheng and X. Shuai, *Adv. Mater.*, 2014, **26**, 8217.

67 F. Alexis, E. Pridgen, L. K. Molnar and O. C. Farokhzad, *Mol. Pharmaceutics*, 2008, **5**, 505.

